EasyChair Preprint

№ 14670

SCAR-UNet: an Improved Res-UNet with Channel and Spatial Attention for Coal Maceral Image Segmentation

Fanqian Meng, Ouli Luo, Hui Ding and Guoping Huo

September 3, 2024

SCAR-UNet: An Improved Res-UNet with Channel and Spatial Attention for Coal Maceral Image Segmentation

Fanqian Meng[1][0009−0008−5663−5837], Ouli Luo[1][0009−0009−7051−799X], Hui Ding[1][0000−0002−1920−7613](✉), and Guoping Huo[2][0009−0006−4504−8149](✉)

[1] College of Information Engineering, Capital Normal University, Beijing, China
dhui@cnu.edu.cn
[2] School of Artificial Intelligence, China University of Mining and Technology-Beijing, China
kuoping@cumtb.edu.cn

Abstract. Coal, as a versatile natural resource fueling various industries, necessitates accurate identification of its maceral components for mining and geological applications. However, automated segmentation of coal macerals remains challenging due to the grayscale similarity between maceral components like liptinite and the background in coal photomicrographs. This study proposes SCAR-UNet, a novel improved network architecture designed specifically for maceral image segmentation. Our approach integrates channel attention, spatial attention, and a novel loss function with the Residual UNet (Res-UNet) architecture, enabling enhanced feature extraction and model performance. Evaluated on a labeled Coal Maceral image dataset comprising 908 annotated images containing vitrinite, inertinite, and liptinite macerals. The widely used Intersection over Union (IoU) and Pixel Accuracy (PA) metrics were utilized for assessing segmentation performance. The proposed SCAR-UNet outperformed state-of-the-art segmentation algorithms.

Keywords: Coal Maceral Segmentation · Residual UNet · Attention Mechanism· Loss Function · Deep Learning.

1 Introduction

As one of the most plentiful fossil fuels on the planet, coal occupies a prominent place in the worldwide energy landscape [1]. Per the guidelines established by the International Committee for Coal and Organic Petrology (ICCP) [2] and the ASTM D2797-13 standard [3] stipulated by the American Society for Testing and Materials (ASTM), three principal categories can be identified within the mineral components of coal: these are (1) Vitrinite, (2) Inertinite, and (3) Liptinite.

Despite advancements, the conventional methodology for coal rock component analysis continues to depend heavily on labor-intensive manual visual inspection techniques [4]. This method is not only devoid of automation but also prone to individual biases [5].

Recent studies have developed numerous image processing and machine learning techniques, enhancing the automation capabilities of coal rock microcomponent segmentation. Li et al. improved the accuracy of target region segmentation in coal and gangue identification based on laser speckle image processing, Gaussian filtering, and adaptive threshold segmentation techniques [6]. Improved U-Net architectures can accurately identify and segment various components in coal maceral micrographs [7]. Convolutional neural networks (CNNs) have successfully analyzed coal maceral granularity features, providing more accurate results than traditional approaches [8]. While these advancements showcase the potential of deep neural networks for automated coal maceral component analysis, existing deep learning models often fall short in capturing intricate structural details and handling the inherent variability present in coal maceral microscopic images. To address the challenges of complex coal maceral microscopic image segmentation, our main contributions are as follows:

1) To better capture intricate details, we propose SCAR-UNet, an improved segmentation network combining Res-UNet with Channel and Spatial Attention mechanisms for effective feature extraction in coal maceral images.
2) A novel loss function, BDL, is designed, combining Binary Cross-Entropy (BCE) loss and Dice loss. The BDL loss function enhances model performance on boundary localization tasks by emphasizing the Dice component and automatically adjusting component weight contributions.
3) Our team has manually annotated a total of 131 coal maceral microscopic images, and subsequently expanded it into a dataset of 908 images through enhancement techniques, which includes Vitrinite, Inertinite, and Liptinite. This high-quality annotated dataset provides valuable data support for coal maceral component segmentation research.

2 Related Works

2.1 Res-UNet Network Model

Ronneberger and his colleagues unveiled the UNet model in 2015 [9]. This model, characterized by an encoder-decoder design, can be effectively trained with a limited set of annotated samples [10]. The Res-UNet model combines ResNet and UNet by integrating residual units before each encoding and decoding layer, enhancing feature propagation and the stability of network training. It can overcome the issue of vanishing gradients and converge rapidly [11].

2.2 Channel Attention and Spatial Attention Mechanism

With the continuous development of deep learning technology, attention mechanisms have gained significant attention due to their remarkable impact on improving model performance. Channel Attention (CA) and Spatial Attention (SA) are two main branches of attention mechanisms. By focusing on channel features and spatial positions of the model respectively, they effectively enhance the accuracy and robustness of segmentation tasks.

Channel attention enhances network performance by emphasizing important features within channels. By assigning different weights to different channels, it significantly improves the representational power of features [12].

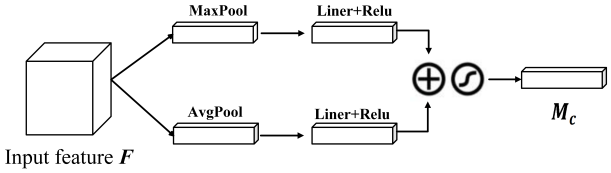

Fig. 1. Channel Attention for Enhanced Feature Representation.

Fig. 1 illustrates the utilization of average pooling and max pooling operations to extract spatial information from feature maps F^c_{avg} and F^c_{max}. These two descriptors are then fed into a shared multi-layer perceptron network, generating a channel attention map $M_c \in \mathbb{R}^{C\times1\times1}$. The network consists of a hidden layer with a size of $\mathbb{R}^{C/r\times1\times1}$, aiming to reduce the number of parameters, where r represents the dimension reduction ratio [13].

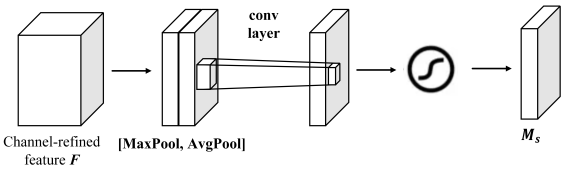

Fig. 2. Spatial Attention for Enhanced Image Segmentation.

Spatial attention enhances the spatial resolution capability of the model by highlighting key regions in the image. It identifies and weights important locations in the image to focus the model's feature processing on specific areas, especially in complex backgrounds or noisy contexts, where this mechanism significantly impacts image segmentation [14]. To obtain spatial attention, average pooling and max pooling operations are first performed along the channel dimension to integrate feature descriptors. Based on the fused descriptors, a convolutional layer is applied to generate the spatial attention map, $M_s \in \mathbb{R}^{C\times1\times1}$, allowing the network to adjust the intensity of specific spatial regions. We employ two pooling operations to integrate the channel information of the feature maps, resulting in two two-dimensional maps: $F^s_{avg} \in \mathbb{R}^{1\times H\times W}$ and $F^s_{max} \in \mathbb{R}^{1\times H\times W}$. Further details and the effectiveness of this model in image segmentation applications in complex environments will be explained in Fig. 2.

3 Methodology

This study is dedicated to addressing the challenges of segmenting coal rock microscopic images, which often exhibit high complexity and heterogeneous distribution. To this end, an advanced deep learning model, SCAR-UNet, has been

developed, and a novel loss function has been introduced to tackle these challenges. By conducting a comprehensive analysis of microscopic image features, this model aims to significantly enhance the accuracy and stability of the image segmentation process.

3.1 Architecture of SCAR-UNet

Selecting and designing an effective network architecture capable of addressing the complexities of image segmentation and data imbalance is crucial for achieving precise image analysis. Addressing the detailed classification and segmentation issues of coal rock microscopic images, this paper introduces the innovative network model, SCAR-UNet. This model integrates spatial attention mechanisms, channel attention, and the powerful features of residual networks, aiming to enhance the precision and efficiency of microscopic image analysis.

To provide a detailed description of the working mechanism of SCAR-UNet and its application in microscopic image segmentation, we will now present its schematic diagram, as shown in Fig. 3.

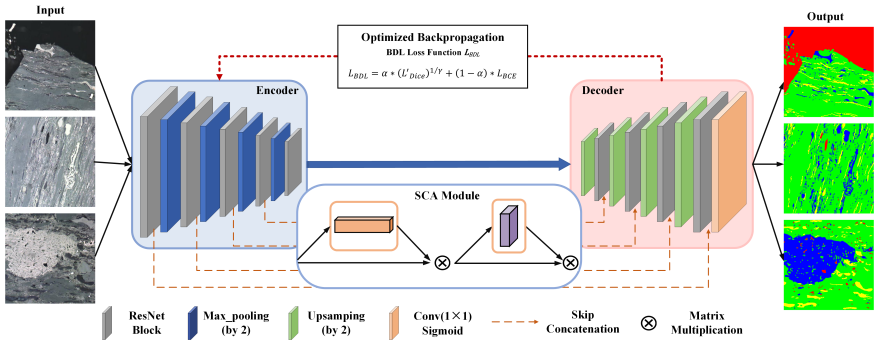

Fig. 3. The architecture of SCAR-UNet with novel loss L_{BDL}.

As can be seen from Fig. 3, the SCAR units employ skip connections, which facilitate selective filtration and transmission of features at various network levels. The SCAR module amalgamates residual units with spatial and channel attention mechanisms, thereby intensifying the model's concentration on prominent features. The incorporation of residual units guarantees that signal propagation remains unimpaired even with the escalation in network depth, safeguarding information throughout multiple network layers. Concurrently, the spatial and channel attention mechanisms adjust the spatial weights of feature maps and accentuate critical channel features respectively. By integrating residual units with channel and spatial attention units, the SCAR-UNet network demonstrates superior efficiency and precision when handling images embedded with complex textures and abundant detail information.

3.2 Innovative Hybrid Loss Function BDL

In the field of image segmentation, the loss function is a critical metric for evaluating model performance. To achieve precise segmentation of coal and rock

micrographs, we propose a novel loss function, BDL, which integrates an improved version of the Dice loss and the binary cross-entropy loss. BDL enhances the model's ability to recognize details, balances segmentation performance, and comprehensively improves image segmentation outcomes. The formula is as follows:

$$L_{BDL} = \alpha * L'_{\text{Dice}} + (1-\alpha) * L_{BCE} \tag{1}$$

In this formula, α is a weight parameter. Higher values of enhance the model's ability to capture edge details [19], while lower values improve the accuracy of pixel classification [18]. Notably, through cross-validation on the training dataset, we ultimately set α to 0.5 to ensure the model's optimal performance in segmenting complex and imbalanced coal rock microscopic images.

The original Dice loss function (L_{Dice}) is based on the Dice coefficient. Its purpose is to maximize the overlap between the predicted segmentation area and the actual segmentation area, making it particularly suitable for handling class imbalances [16]. The Dice loss function is defined as follows:

$$L_{\text{Dice}} = 1 - \frac{2\sum_i^N p_i g_i + \epsilon}{\sum_i^N p_i + \sum_i^N g_i + \epsilon} \tag{2}$$

Where p_i is the predicted probability for each pixel i , g_i is its true label (0 or 1), N refers to the total number of pixels in the image, and ϵ is a small constant used to prevent the denominator from becoming zero.

Although the original Dice loss function performs well in image segmentation tasks, it may not be sufficiently sensitive for some specific scenarios, such as detecting small objects or achieving precise segmentation of edges [17]. Therefore, we introduced a power factor γ. The expression for the improved Dice loss function is as follows:

$$L'_{\text{Dice}} = (L_{\text{Dice}})^{1/\gamma} \tag{3}$$

By finely tuning the hyperparameter γ to $\frac{4}{3}$ through ten-fold cross-validation on the training set, we optimized the sensitivity of the improved Dice loss function. This adjustment enhances the model's ability to detect and segment complex regions in image data. The increased penalty weights for challenging areas guide the model in recognizing difficult regions, providing a flexible error penalty mechanism. This design mitigates the impact of class imbalances in coal rock microscopic images, improving the model's robustness and segmentation accuracy.

In Equation (3), L_{BCE} denotes the Binary Cross Entropy (BCE) loss function. It measures the discrepancy between predicted probabilities and target labels, compelling the model to make accurate classification decisions for each pixel [15]. Its mathematical formula is defined as follows:

$$L_{BCE} = -\frac{1}{N}\sum_{i=1}^{N}\left[y_i \cdot \log\left(\hat{y}_l\right) + \left(1-y_i\right) \cdot \log\left(1-\widehat{y}_l\right)\right] \tag{4}$$

Where N is the total number of samples, y_i is the true label of the ith sample. In binary classification problems, y_i takes the value of 0 or 1. $\hat{y}_l$ represents the predicted probability of the ith sample. When the true label y_i is 1, the term $y_i \cdot \log\left(\hat{y}_l\right)$ is active. When y_i is 0, the term $\left(1-y_i\right) \cdot \log\left(1-\widehat{y}_l\right)$ is active.

4 Experiment

4.1 Construction of Datasets

Due to the current lack of publicly available annotated datasets for coal surface microscopic images, this study has constructed a dataset suitable for training and evaluating deep learning models using annotated images obtained from the internet [20]. As illustrated in Fig. 4, the top row shows examples of the acquired annotated coal maceral microscopic images. Image restoration techniques were applied, yielding the clean images shown in the bottom row of Fig 4.

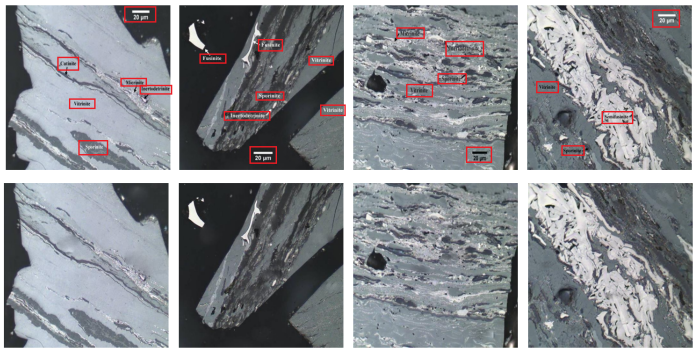

Fig. 4. Samples of Coal Maceral Microscopic Annotated Image (Top Line) and Annotated Dataset (Bottom Line).

Using the calibration tool [21], we manually annotated 131 images in the dataset, selecting 20 of them as the test set. The remaining 111 images were augmented to 888 images through geometric transformations such as rotation and noise injection. Figure 5 shows an example of the annotated coal petrographic images. We used specific color coding to distinguish different categories: red represents the background, green represents the vitrinite group, blue represents the inertinite group, and yellow represents the liptinite group. We employed a decomposed approach, transforming the multi-class problem into several binary classification problems.

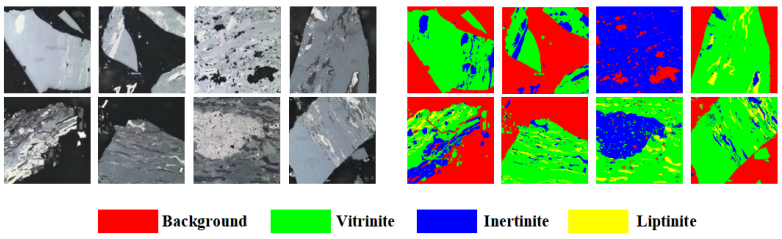

Fig. 5. Coal Maceral Image Samples: Original Images (Left), Label Images (Right).

4.2 Details of Implementation and Metrics for Evaluation

The evaluation of training results in this study employs Intersection over Union (IoU), Pixel Accuracy (PA), Recall, and the Dice coefficient. IoU reflects the model's ability to accurately delineate the target boundaries. PA provides insights into the model's overall performance across all classes. Recall calculates the proportion of true positives correctly identified among all actual positives. The Dice coefficient evaluates the accuracy of the model in identifying the overlap between the predicted target areas and the actual target areas. The specific calculation expressions are as follows:

$$IoU = \frac{V_{pred} \cap V_{gt}}{V_{pred} \cup V_{gt}} \tag{5}$$

$$PA = \frac{TP + TN}{TP + TN + FP + FN} \tag{6}$$

$$Recall = \frac{TP}{TP + FN} \tag{7}$$

$$Dice = \frac{2 * TP}{2 * TP + FP + FN} \tag{8}$$

Where V_{pred} represents the predicted result and V_{gt} represents the ground truth. TP represents the true positive, TN represents the true negative, FP represents the false positive, and FN represents the false negative.

4.3 Comparative Analysis of Loss and Pixel Accuracy

This section presents a comparative analysis of the loss and pixel accuracy (PA) for four distinct segmentation models: Res-UNet, CAR-UNet, SAR-UNet, and SCAR-UNet. The loss curves are illustrative of the model convergence behavior during training, while the PA curves reflect the precision of pixel-level identification across the testing dataset.

As shown in the left column of Fig. 6, the loss curves reveal a significant decrease in the loss values for all models during the initial phase of training, indicating that the selected learning rate facilitated an effective gradient descent process. Subsequently, the loss curves gradually stabilized, suggesting that the models began to converge, demonstrating the appropriateness of the set learning rate. The red curve represents the SCAR-UNet model, which converged at the fastest rate and ultimately achieved the lowest loss value among all models. This indicates the SCAR-UNet model's highly effective capability in extracting and classifying features from coal rock microscopic images. Such rapid convergence and low loss values typically signify that the model is highly stable during the learning process, capable of capturing patterns and correlations in the data more accurately, thereby enhancing the model's generalizability and practicality.

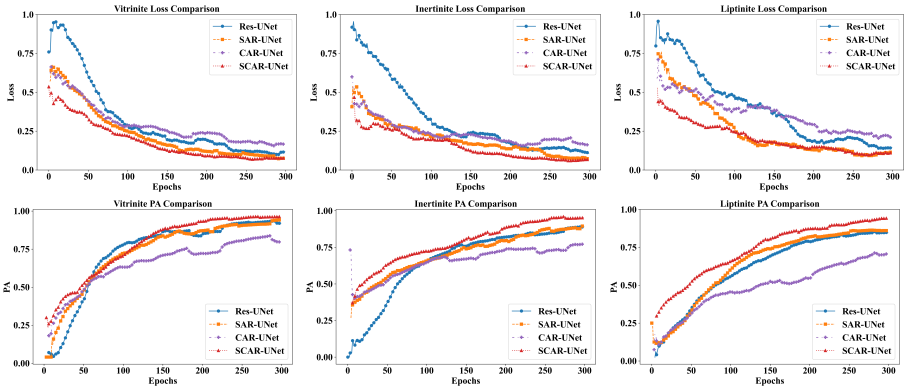

Fig. 6. Comparative Analysis of Loss(left) and PA(right) for four Models during Training.

From the right column of Fig. 6, it can be observed that the red curve not only shows the fastest growth rate but also ultimately achieves the highest PA value, demonstrating the exceptional performance of the SCAR-UNet in the task of coal rock microscopic image segmentation. This performance reflects the model's high efficiency in accurately identifying and segmenting various coal rock components, ensuring high classification accuracy and detail restoration.

4.4 Results and Discussion

Ablations In the ablation study, We conducted six models: RES-UNet, Res-UNet with BDL loss, Res-UNet with spatial attention(SAR-UNet), Res-UNet with channel attention(CAR-UNet), SCAR-UNet, and SCAR-UNet with BDL loss, as shown in Table 1, where the best results are highlighted in bold.

According to the table, the SCAR-UNet+BDL model exhibited optimal performance for Inertinite and Liptinite across the metrics PA, IoU, Recall, and Dice. The respective values for these four evaluation metrics for Inertinite/Liptinite were 0.985/0.922, 0.836/0.928, 0.845/0.925, and 0.910/0.962. The results indicate that the SCAR-UNet+BDL model possesses superior segmentation capabilities for complex coal rock micro-images. From the PA, IoU, and Dice metrics, it is evident that SCAR-UNet predicts Vitrinite most effectively. This can be attributed to the largest dataset proportion of Vitrinite, while BDL significantly enhances prediction outcomes for Inertinite and Liptinite, which have smaller dataset representations. Among the three coal rock categories, based on the maximum values of the four metrics, Vitrinite generally ranks higher than Liptinite and Inertinite, a result stemming from Vitrinite's highest representation in the dataset, whereas Inertinite has the lowest.

Comparison Experiments To demonstrate the advantages of incorporating spatial and channel attention mechanisms as well as the BDL loss function in our model, we conducted a series of comparative experiments. We selected four

Table 1. Ablation Experiment: Comparison of the Prediction Results for Three Categories of Coal Maceral Images.

Metrics / Models		RES-UNet	RES-UNet+BDL	SAR-UNet	CAR-UNet	SCAR-UNet	SCAR-UNet+BDL
PA	Vitrinite	0.972	0.975	0.978	0.982	**0.989**	0.986
	Inertinite	0.969	0.980	0.978	0.982	0.981	**0.985**
	Liptinite	0.980	0.982	0.981	0.983	0.991	**0.992**
IoU	Vitrinite	0.918	0.945	0.940	0.967	**0.976**	0.970
	Inertinite	0.791	0.803	0.823	0.829	0.830	**0.836**
	Liptinite	0.882	0.909	0.910	0.921	0.922	**0.928**
Recall	Vitrinite	0.920	0.945	0.940	0.960	0.965	**0.970**
	Inertinite	0.790	0.810	0.830	0.840	0.840	**0.845**
	Liptinite	0.880	0.905	0.910	0.920	0.920	**0.925**
Dice	Vitrinite	0.957	0.972	0.969	0.983	**0.988**	0.985
	Inertinite	0.883	0.890	0.902	0.908	0.909	**0.910**
	Liptinite	0.937	0.952	0.953	0.959	0.960	**0.962**

models for this purpose: U-Net, AG-UNet with attention gates, Res-UNet with residual connections, and DeepLab-V3+ (DL-V3+).

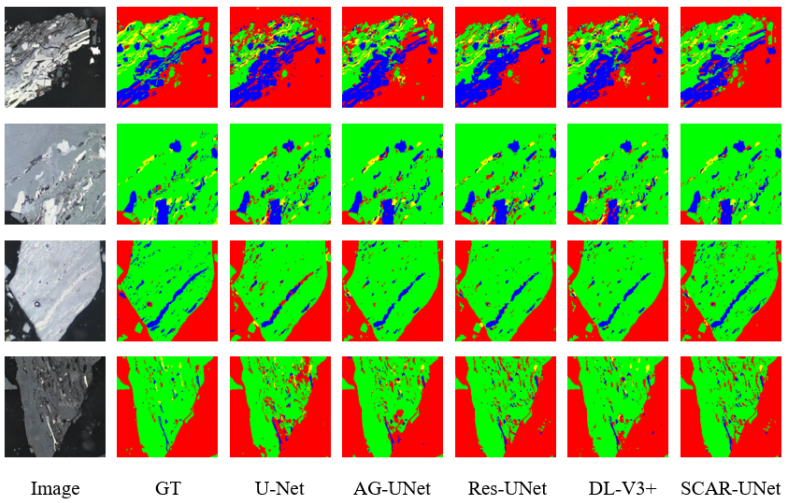

Fig. 7. Comparison of Segmentation Results Among Four Models: U-Net, AG-UNet, Res-UNet, DL-V3+ and SCAR-UNet.

These models were used to perform semantic segmentation predictions on the test set. To thoroughly evaluate the segmentation performance of the models, we continued to use PA, IoU, Recall, and Dice as the core evaluation metrics.

The comparative results are presented in Table 2, where the best results are highlighted in bold. The segmentation outcomes of the four models on coal rock micro-images can be visualized in Fig. 7.

From Fig. 7, it can be seen that the segmentation results obtained by SCAR-UNet are closest to the ground truth images. Compared to the SCAR-UNet model, the DeepLab-V3+ and AG-UNet model's segmentation results lack some fine details and occasionally fail to fully recognize certain features. In contrast, the U-Net model's predictions often contain more errors, such as predicting extra coal rock components or missing some areas.

Table 2. SCAR-UNet Model Compared with Four Classic Models.

Metrics / **Models**		U-Net	AG-UNet	Res-UNet	DL-V3+	SCAR-UNet(ours)
PA	Vitrinite	0.964	0.974	0.972	0.967	**0.989**
	Inertinite	0.953	0.970	0.969	0.961	**0.981**
	Liptinite	0.987	0.988	0.990	0.989	**0.991**
IoU	Vitrinite	0.917	0.928	0.918	0.920	**0.976**
	Inertinite	0.796	0.786	0.791	0.798	**0.830**
	Liptinite	0.872	0.901	0.882	0.890	**0.922**
Recall	Vitrinite	0.921	0.932	0.920	0.923	**0.965**
	Inertinite	0.792	0.788	0.790	0.801	**0.840**
	Liptinite	0.879	0.905	0.880	0.891	**0.920**
Dice	Vitrinite	0.925	0.938	0.957	0.927	**0.988**
	Inertinite	0.798	0.790	0.883	0.805	**0.909**
	Liptinite	0.881	0.906	0.937	0.895	**0.960**

From Table 2, we can observe that among the five models, SCAR-UNet model exhibited the highest PA, IoU, Recall, and Dice scores across all three coal rock categories. Specifically, for Vitrinite/Inertinite/Liptinite, SCAR-UNet showed improvements over Res-UNet by 1.7%/1.2%/0.1% in PA, 5.8%/3.9%/4% in IoU, 4.5%/5%/4% in Recall, and 3.1%/2.6%/1.3% in Dice respectively. Compared to DeepLab-V3+, SCAR-UNet demonstrated enhancements of 2.2%/2%/0.2% in PA, 5.6%/3.2%/3.2% in IoU, 3.2%/3.9%/2.9% in Recall, and 6.1%/10.4%/6.5% in Dice. These results indicate that the SCAR-UNet model possesses outstanding performance in handling complex coal rock micro-image segmentation tasks. This exceptional performance can be attributed to the integration of spatial and channel attention mechanisms within the model structure. Additionally, the results obtained from our calibrated dataset with DeepLab-V3+ were superior to those reported in the referenced paper [22], with PA/IoU scores for Vitrinite of 0.94/0.87, Inertinite of 0.79/0.71, and Liptinite of 0.95/0.83. This also proves the reliability and accuracy of the dataset calibrated in this study.

5 Conclusion

Segmenting and analyzing coal rock components in microscopic images play a crucial role in characterizing coal properties and optimizing the coal utilization process. However, existing methods often face difficulties in accurately depicting complex structural details and handling the variability of coal rock images. To address these challenges, this paper proposes a novel deep learning approach for coal rock image segmentation based on an improved attention residual U-Net (SCAR-UNet) architecture. Specifically, we have incorporated channel attention and spatial attention into the Res-UNet, mechanisms that help the model more accurately focus on key features within the images, thereby improving segmentation accuracy. Additionally, we designed a new loss function, BDL, which is a weighted combination of binary cross-entropy loss and mean intersection-over-union loss. Compared to other state-of-the-art semantic segmentation models, our approach achieves higher pixel accuracy (PA) reaching 98.8%, and mean intersection-over-union (IoU) reaching 91.6%, significantly outperforming existing technologies.

Although the proposed method has already shown promising results, further research could focus on integrating advanced attention mechanisms or exploring multi-task learning frameworks to achieve simultaneous segmentation of multiple categories and classification of coal rock components. Moreover, integrating domain-specific knowledge or leveraging weak supervision techniques could enhance model performance and reduce dependence on large amounts of labeled data.

References

1. Guatame, C., Rincón, M.: Coal petrology analysis and implications in depositional environments from upper Cretaceous to Miocene: a study case in the Eastern Cordillera of Colombia. Int J Coal Sci Technol, **8**(1), 1–28 (2021).
2. Kwiecińska, B., Petersen, H.: Graphite, semi-graphite, natural coke, and natural char classification-iccp system. Int J Coal Geol, **57**(2), 99–116 (2004).
3. ASTM: Standard Test Method for Microscopical Determination of the Maceral Composition of Coal. ASTM D2799 (2013b).
4. Wang, Y., Bai, X., Qu, S.: Research Progress of Automatic Identification Technology of Coal and Rock Microscopic Components. Coal Quality Technology, **36**(01), 49–57 (2021).
5. Młynarczuk, M., Górsczyk, A., Ślipek, B.: The application of pattern recognition in the automatic classification of microscopic rock images. Computers Geosci, **60**, 126–133 (2013).
6. Li, H., Wang, Q., Ling, L., Lv, Z., Liu, Y., Jiao, M.: Research on recognition of coal and gangue based on laser speckle images. Sensors, **23**(22), 9113 (2023).
7. Wang, H., et al.: Intelligent identification of maceral components of coal based on image segmentation and classification. Appl Sci, MDPI (2019).
8. Fan, J., et al.: Macerals particle characteristics analysis of tar-rich coal in northern Shaanxi based on image segmentation models via the U-Net variants and image feature. Fuel, Elsevier (2023).

9. Ronneberger, O., Fischer, P., Brox, T.: U-Net: Convolutional Networks for Biomedical Image Segmentation. Lecture Notes in Computer Science, vol. 9351, 234–241, Springer, Cham (2015).
10. Ono, K., Iwamoto, Y., Chen, Y.W., Nonaka, M.: Automatic Segmentation of Infant Brain Ventricles with Hydrocephalus in MRI Based on 2.5D U-Net and Transfer Learning. J Image Graphics, **8**(2), 42–46 (2020).
11. Zhou, J., Lu, Y., Tao, S., Cheng, X., Huang, C.: E-Res U-Net: An Improved U-Net Model for Segmentation of Muscle Images. Expert Syst Appl, **166**, 114060 (2021).
12. Azizpour, H.: Building Extraction from High-Resolution Aerial Imagery Using a Generative Adversarial Network with Spatial and Channel Attention Mechanisms. Remote Sensing, **11**(8), 917 (2023).
13. Woo, S., Park, J., Lee, J.Y., et al.: CBAM: Convolutional Block Attention Module. Proc Eur Conf Comput Vis (ECCV), (2018).
14. Ates, C.G., et al.: Dual Cross-Attention for Medical Image Segmentation. arXiv preprint arXiv:2303.17696 (2023).
15. Long, J., Shelhamer, E., Darrell, T.: Fully Convolutional Networks for Semantic Segmentation. Proceedings of the IEEE Conference on Computer Vision and Pattern Recognition, 3431–3440 (2015).
16. Jha, S., Kumar, R., Priyadarshini, I., Smarandache, F., et al.: Neutrosophic Image Segmentation with Dice Coefficients. Measurement, Elsevier (2019).
17. Zhao, R., Qian, B., Zhang, X., Li, Y., Wei, R., et al.: Rethinking Dice Loss for Medical Image Segmentation. Proceedings of the IEEE Conference on Data Mining and Big Data (DMBD), IEEE (2020).
18. Pezzano, G., Ripoll, V.R., Radeva, P.: CoLe-CNN: Context-learning Convolutional Neural Network with Adaptive Loss Function for Lung Nodule Segmentation. Computer Methods and Programs in Biomedicine, vol. 198, 105792 (2021).
19. Zhou, X., Li, Z., Tong, T.: DTSC-Net: Semi-supervised 3D Biomedical Image Segmentation through Dual-teacher Simplified Consistency. IEEE International Conference on Image Processing (ICIP), 1429–1434 (2022).
20. U.S. Geological Survey: ASTM Coal Maceral Classification. [Online]. Available: `https://energy.usgs.gov/PhotoAtlas/default.aspx?aid=3`. [Accessed: 20-Jan-2023].
21. APEER by ZEISS: APEER Viewer. [Online]. Available: `https://www.apeer.com/viewer/?datasetId=7201a323-2946-45f3-90f0-a0c3b4cb73c7&mlwf`. [Accessed: 01-Oct-2023].
22. Wang, Y., Bai, X., Wu, L., Zhang, Y., Qu, S.: Identification of maceral groups in Chinese bituminous coals based on semantic segmentation models. Fuel, **308**, 121844 (2022).